Characterization of p$^+$-n Junctions and a Quasi-One-Dimensional Structure Fabricated by Low-Energy Focused Ion Beam

Peerasak Chantngarm[1], Non-member

ABSTRACT

The electrical properties of implanted p$^+$ layers, shallow p$^+$-n junctions, and a quasi-one-dimensional structure fabricated without masks by 20-keV Ga$^+$ focused ion beam (FIB) on crystalline Si substrates were investigated in details. The distribution profile from SIMS showed discrepancies from LSS theory, which is considered to be the results of low beam energy and high beam current density. From Hall effect measurements, the Hall drift mobility was 131 cm^2 / V-sec, which is 62% of the projected value due to remained defects after annealing. The $I-V$ characteristics of p$^+$-n junctions illustrated four distinct regions in the forward bias region and rising saturation current in the reverse bias region. Higher than expected leakage current is considered to be the results of residue damages after annealing. For the first time, the resistance of a quasi-one-dimensional structure was investigated. The resistance is 1.1×10^9 , which is 647 times higher than the projected value. The cause of this phenomenon is considered to be the combined effects of interfacial roughness, the residue damages, and the shape of the structure.

Keywords: Focused ion beam, p$^+$-n junctions, SIMS, $I-V$ characteristics, quasi-one-dimensional structure

1. INTRODUCTION

As MOSFETs are scaled down to the deep submicron regime, many problems are encountered. Short-channel effect, which causes many unwanted phenomena such as lower absolute value of threshold voltage, is one of serious problems among them. With an insight from the scaling rule, it has been known that the short-channel effects could be avoided by forming shallow p-n junctions for the sources and drains of MOS devices [1-2]. Low-energy ion implantation is one of widely used methods, since it has many advantages over diffusion technology [3-4]. First, it is a low temperature process. Second, the distribution profile of implanted dopant could be more easily and accurately controlled with the implanting time and the energy of ion beam. At the same time, the efforts to scale down MOSFETs and the advance in fabrication technology have created many kinds of new Si devices. One of them is quantum wire devices [5-6].

On the other hand, focused ion beam (FIB) has gained popularity during the past decade due to its versatility. With the beam diameter of about 0.1 μm, in the case that heavy ions such as Ga$^+$ are utilized with long enough exposure, it could also be used in maskless etching. Therefore, FIB has become an important tool for the failure analysis and yield improvement. Moreover, maskless ion implantation has also become possible. While the conventional ion implantation technique is still the mainstream, FIB could be used to complement in some areas, such as channel doping [7-8]. Using low-energy FIB will also allow us to form shallow p-n junctions to avoid short-channel effects without using mask. Moreover, FIB can be applied to make quasi-one-dimensional structure masklessly.

Although, the idea of using low-energy FIB to form shallow p-n junctions has been investigated in the past, the detailed studies on the $I-V$ characteristics of the junctions had not been done yet [9-10]. Since FIB has large beam current density, more defects are expected along with other possible unknown side effects, which in turn would affect the $I-V$ characteristics. Therefore, there are clear benefits in deeper understanding in the electrical characteristics of the p-n junctions formed by this method. Moreover, to the best of our knowledge, there is no report on attempt of quasi-one-dimensional structure fabrication by FIB.

In this study, we focused on the detailed investigation of $I-V$ characteristics of the implanted p^+ layers and the p$^+$-n junctions on crystalline Si substrate fabricated by 20-keV Ga$^+$ FIB at the room temperature. Furthermore, a quasi-one-dimensional structure was also fabricated and the electrical characteristics were investigated for the first time. The rest of the paper is organized as follows. Section 2 briefly introduces the theories related to our experiments. Section 3 briefly describes the experimental procedures. Section 4 shows the experimental results, and the analysis. We draw out the conclusions in section 5.

Manuscript received on February 17, 2008 ; revised on July 27, 2008.

[1] The author is with Electronics and Telecommunication Engineering Department, Pathumwan Institute of Technology, Bangkok, Thailand, E-mail: cpeerasak@yahoo.com

2. THEORY

2.1 Stopping Mechanisms

When charged particles are implanted into solids, they collide with atoms of the target and lose energy until stop. There are two kinds of stopping mechanisms for ions implanted into targets, nuclear stopping and electronic stopping. The dominant mechanism is determined by the mass and the energy of the accelerated ions, as well as the mass of the target atoms. In the case of implanting 20 -keV Ga^+ into Si, the major part of energy loss is due to nuclear stopping which contributes to cascade collision and sputtering, which induces a lot of damages [11].

2.2 Junction Depth

According to the LSS theory [12], the implanted ions in amorphous medium have a Gaussian range distribution around an average projected range R_p, with a standard deviation ΔR_p. Furthermore, when the ion dose is N, the ion density at the depth x could be expressed by the following equation [11].

$$N(x) = \frac{N}{\Delta R_p \sqrt{2\pi}} \exp\left[-\frac{(x-R_p)^2}{2\Delta R_p^2}\right] \tag{1}$$

In the case that ions are implanted to form a p-n junction, (1) could be used along with the carrier concentration of substrate to calculate the as-implanted junction depth. However, there are many secondary effects, such as channeling effects, which could affect the junction depth. Furthermore, the real p-n junctions need to be annealed to repair lattice damages, and the diffusion during the process would affect the junction depth, too.

2.3 $I-V$ Characteristics of p-n Junctions

An important tool in the analysis of p-n junctions is the $I-V$ characteristics plotted in semi-log scale. Taking secondary effects into account, the real total current of a p-n junction could be expressed as follows:

$$I = I_s\left[\exp\left(\frac{q(V-Ir_s}{nkT}\right)-1\right] \tag{2}$$

where I_S is the saturation current, q is the magnitude of electron charge, V is the applied voltage, k is the Boltzmann's constant, and T is temperature, r_s is the series resistance and n is the diode ideality factor. In theory, n varies between 1 and 2 on each region in the forward bias diode, while the ideality factor equals to 1 in the ideal diode.

When we plot the forward $I-V$ characteristics of p-n junctions in semi-log scale, it could be divided into four distinct regions [13-15]. In the first region where $Ir_S \ll V \ll nkT/q$, the following approximation could be used.

$$\exp\left(\frac{qV}{nkT}\right)-1 \approx \frac{qV}{nkT} \tag{3}$$

Therefore, the total current in this region linearly depends on the applied voltage as follows:

$$I = I_S\left(\frac{q}{nkT}\right)V \tag{4}$$

For the region that $V \gg nkT/q$, the total current is dominated by the recombination current in space-charge region (scr) at lower current, where the ideality factor is 2. On the other hand, at higher current, the total current is mainly diffusion current, where the ideality factor is 1. The last region is where the forward bias voltage is higher than 1 volt. In this region, the current increases at a slower rate and the p-n junction behaves like an ohmic resistor. This is due to the combined effects between the high level injection and series resistance.

Regarding the $I-V$ characteristics with reverse bias voltage, the saturation current in the real p-n junction could increase almost linearly with the square root of reverse bias voltage. This is due to carrier generation within the transition region, which increases with the width of the transition region increasing with the reverse bias [16].

3. EXPERIMENTAL

Czochralski (CZ) grown n-type silicon substrates of (100) orientation and 3-7 Ωcm of resistivity were used. RCA cleaning technique was carefully performed to remove contamination from the substrates prior to using them in experiments. Silicon dioxide layer of 150-nm thickness was deposited on the top of the substrates with dry thermal oxidation technique. The thickness of the SiO_2 layer was measured with ellipsometry method. Then it was etched with buffered HF solution to obtain implant area. This SiO2 layer was used as a marker for the ion implantation area, mask for the implantation at the selected area, and also as an insulation layer between electrodes and the substrate. Positive photoresist was used for the patterning of the structure. The FIB system used in this study is model EFIB-2000S from Eiko Engineering. The ion source was needle-type liquid metal ion source (LMIS) which could provide relatively stable Ga^+ ions beam. Fig. 1 illustrates the cross section of the structure.

In this study, three kinds of experiments have been done. First, the junction depth was measured by using stain method and the distribution profile of dopant was obtained by Secondary Ion Mass Spectrometry (SIMS) technique. Four kinds of specimens were prepared for this experiment as summarized in Table 1. Regarding the ion implantation, 20-keV gallium ions were raster-scanned with dose of 1×10^14

/cm^2 without screen oxide. The implant area in the first and the second experiment is 1.0 × 0.8 mm^2. The beam current was 40 pA, and the beam diameter was about 0.1 μm. Here, the beam diameter was derived from beam energy and beam current based on the specification from the manufacturer [17]. For the 7° off-axis implantation, the substrate was tilted to < 110 > direction by 7 degrees to avoid channeling effect. The anneal condition used was 800 °C, 30 minutes in furnace in a dry Ar ambient.

To measure the junction depth with stain method, each specimen was glided off for 3 degrees at the implant area as illustrated in Fig. 2, and was put in stain liquid which consists of HF, HNO_3 and CH_3COOH. If a p-layer is formed, the difference in the brightness between the n-layer and the p-layer can be noticed by a Nomarski microscope, which allows us to measure the thickness of the formed p^+-layer and the junction depth. In addition to the stain method, SIMS technique was used in order to find out the distribution profiles of dopant.

Table 1: *Summary of the implantation and annealing conditions used in each experiment.*

Experiments	Sample No.	Conditions of specimens used
Stain method	1	on-axis, annealed
	2	on-axis, as-implant
	3	7 °off-axis, annealed
	4	7 °off-axis, as-implant
SIMS	1	on-axis, annealed
	2	on-axis, as-implant
$I-V$ characteristics		7 °off-axis, annealed
Quasi-one-dimensional structure		7 °off-axis, annealed

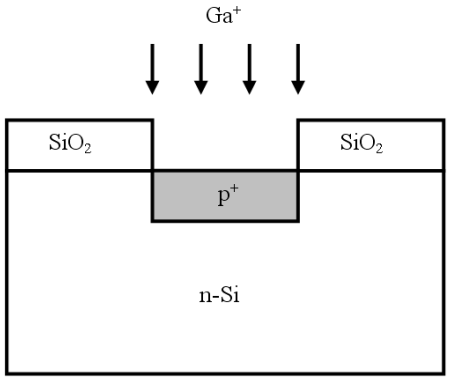

Fig.1: *A cross-sectional view of the implanted area.*

In the second experiment, the $I-V$ characteristics of the p^+-n junctions were measured, and the Hall effect measurement was done. The implantation and anneal condition used in this experiment is shown in

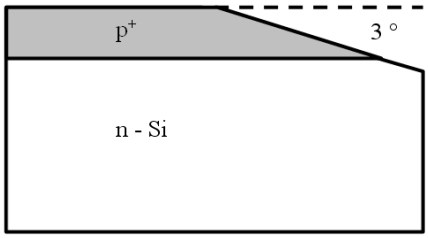

Fig.2: *A cross-sectional view of the specimen prepared for stain method.*

Table 1. To measure the $I-V$ characteristics, ohmic-contact electrodes were formed by using Al/Ti as the electrode for the p^+-layer and AuSb as the electrode for the n-layer. This is because the Ti would form the low resistivity TiSi2 silicide, while AuSb would form an n^+ layer at the surface of Si, which result in very good ohmic contacts [18]. For alignment purpose during the photolithography process, 0.2-μm-deep registration marks were formed into the Si substrate by reactive ion etching (RIE) with CF_4 + O_2 plasma. The metallization was done with evaporation technique in a vacuum of 3×10^{-6} Torr followed by sintering with Xe flash lamp at 410 °C for 1 minute in nitrogen ambient. Finally, the $I-V$ characteristics were measured at the room temperature.

In the last experiment, a narrow line, which is considered as a quasi-one-dimensional structure, was drawn with FIB as shown in Fig. 3. In this experiment, in addition to implanting with line-mode, implantation was also done with area-mode at both sides of the line to form contact layers for the electrical measurement. The length of the line is 0.8 cm, while the distance between the contact layers is 0.5 cm, to make sure that the line and the contact layers are connected to each other. After annealing, electrodes were formed at the both sides of the line with the same process as in the previous experiment. Finally, the resistance of the structure was measured.

4. RESULTS AND DISCUSSION

4.1 Junction Depth and Distribution Profile

The as-implant junction depth of p-n junctions in our experiment, using 20-keV Ga^+ ion implantation with the dose of 1×10^{14} /cm^2 into Si substrate with 3-7 Ω-cm of resistivity, was calculated from (1). In this case, the average projected range R_p is 0.0162 μm, and the standard deviation ΔR_p is 0.0062 μm [19]. From the resistivity of the substrate, we are able to derive the carrier concentration to be 1×10^{15} /cm^3 [20]. Therefore, the junction depth is projected to be 45 nm in the ideal situation.

Table 2 summarizes the junction depth measured by the stain method. The results showed that the junction depth after annealing was 560 nm for on-axis implantation, and 410nm for the 7 °off-axis implan-

Table 2: *Junction depths measured by stain method.*

	as-implant	annealed
on-axis implantation	N/A	560 nm
7 °off-axis implantation	N/A	410 nm

tation. The junction depth of the as-implant specimens could not be measured by the stain method due to weak contrast between the implanted layers and the substrates. This might have happened because the dopant in the implanted layers was not activated by annealing yet. Therefore, there is extremely small number of carriers in the implanted layers of as-implant samples. This made the etching rate at the implanted layers very small and almost the same as at the substrates. So the contrast between the two layers was not big enough to be noticed. Fig.4 shows the topography of the annealed specimen with 7 °off-axis implantation observed by Nomarski microscope.

Secondary-ion mass spectrometry (SIMS) was also used to obtain the distribution profiles. Fig.5 illustrates the results from SIMS with the solid line, and the projected distribution profile from LSS theory with the dashed line. The comparison shows that the real distribution profiles of dopant have long tails much deeper into the substrate than the profile projected by the theory, especially after annealing. This is consistent with the results from the stain method, which showed that the junction depth is deeper after annealing.

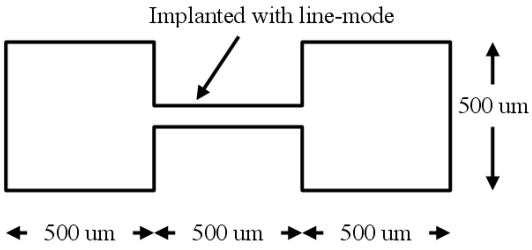

Fig.3: *Top view of the diagram of the narrow line structure.*

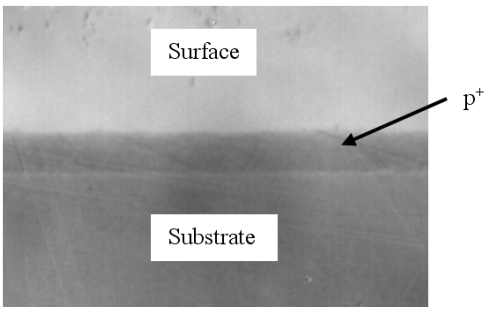

Fig.4: *Topography of the annealed specimen with 7 °tilt-angle implantation.*

The discrepancy in junction depths between our

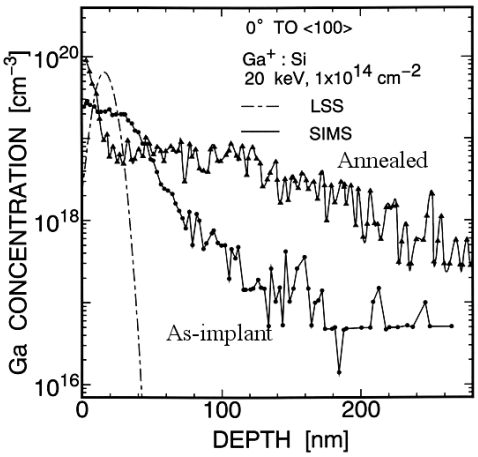

Fig.5: *Distribution profiles of dopant obtained by SIMS and LSS theory.*

experimental results and the projection from theory is considered to come from the long tail due to channeling effects, diffusion, and sputtering. On one hand, it has been known that the LSS theory, which is a physically base model, does not properly include electronic stopping model. Therefore, it cannot predict the channeling effects well enough like other more developed model [21], especially when low beam energy is used. On the other hand, it is obvious that the distribution profile was greatly affected by both primary and secondary short channel effects, which came from many reasons. First, there is no preamorphizing implant (PAI) [22]. Second, the low carrier concentration of the substrate, $1x10^{15}$ /cm^3, allows more room for the long tail. Third, the low implant energy might magnify the secondary channeling effects, due to the increase of angular acceptance to the channel [23]. Here, the secondary channeling effect is the channeling that happens at greater depth with lower concentration than the primary channeling effect. Although, Ga+ has a high ability to damage the silicon and amorphize the substrate, channeling can still occur during the early stage of implantation, when the amorphous layer was not completely formed yet.

In addition to channeling effects, diffusion might also play a role in the long tail of the distribution profile. First, the enhanced diffusion of dopant might happen due to the interaction of point defects with the diffusing gallium atoms [24]. Second, since FIB has higher beam current density than conventional ion beam, it is expected that more heat would be generated, which might cause more diffusion. Another reason of the long tail is considered to be the sputtering which wears some part of the top layers of the specimens [25]. One more interesting characteristic could be observed from Fig. 5. Both as-implant and annealed specimens shows the highest concentration of gallium at the surface, which contradicts the projection from LSS theory. This might be the re-

sults of the redeposition effect of sputtered gallium and the precipitation of gallium [25].

4.2 $I-V$ Characteristics of the p^+-n Junctions

Prior to analyze the I-V characteristics, Hall effect measurement was done by using the van der Pauw technique on a specimen with on-axis implantation. Based on the junction depth of 560 nm, the results are as following. The implanted layer is p-type, the carrier concentration is 2.9×10^{17} /cm^3, the resistivity is 0.16 -cm and the Hall drift mobility is 131 cm^2 / V-sec. While the Hall drift mobility in silicon with impurity concentration of 2.9×10^{17} /cm^3 is expected to be about 210 cm^2 / V-sec, the result from the measurement is about 62% of that value [26]. This result means that there were defects still remained inside the implanted layer after annealing.

Fig.6 shows the current-voltage characteristics of the p-n junction in linear scale at very small forward bias voltage region, from 0.00 V to 0.16 V. The result indicates linearity, which agrees very well with (4) for the region 1 of $I-V$ characteristic. Fig.7 illustrates the $I-V$ characteristics of the same p-n junction in semi-log scale, for both forward and reverse bias voltages. The shape of the $I-V$ characteristics illustrates region 2, 3 and 4 of the p-n junction as described in Section 2.3.

In regard to the $I-V$ characteristics with reverse bias voltage, the Fig.7 shows rising saturation current, which is qualitatively consistent with the theory described in Section 2.3. However, the value of the saturation current is about 10^{-4} A/cm^2 at the reverse bias of 5V, which is considered to be high [4]. This high saturation current is considered to be the results of the defects remained after annealing, which in turn acted as generation-recombination sites. Better annealing technique such as RTA might help alleviate this problem. This result is consistent with the lower than expected Hall drift mobility.

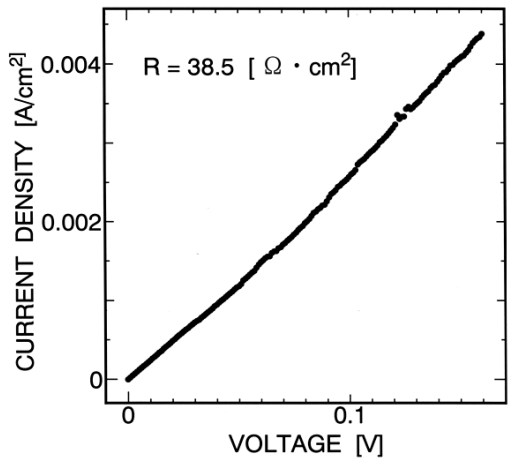

Fig.6: *$I-V$ characteristics of the p-n junction at very low forward voltage in linear scale.*

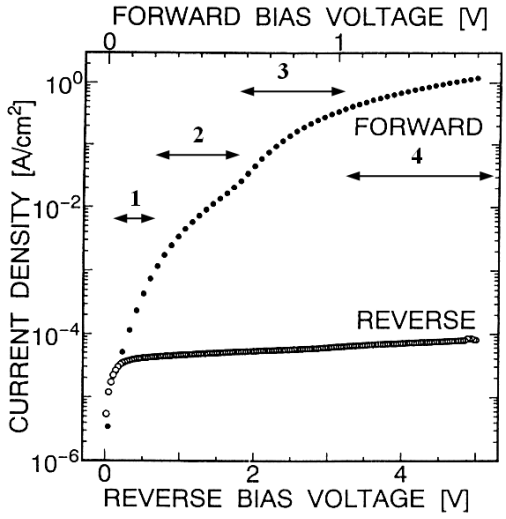

Fig.7: *$I-V$ characteristics of the p-n junction dose of 1×10^{14} /cm^2 in semi-log scale.*

4.3 Quasi-One-Dimensional Structure

Fig.8 shows the surface topography of the narrow line obtained by Nomarski microscope after being put in stain liquid. Fig.9 depicts the $I-V$ characteristics of the narrow line structure in the last experiment. From the resistivity obtained by Hall effect measurements, the junction depth obtained from the first experiment, and the size of the structure, the resistance was projected to be 1.7×10^6 Ω. However, the $I-V$ characteristics in Fig.9 shows that the resistance of the structure is 1.1×10^9 Ω.

Although there was a report on the quantum effects in quasi-one-dimensional structure [27], the line width considered as a quantum wire structure is 0.1 um or lower. However, the line width in our study is about 1 um, so it is too large for quantum effects to happen. Therefore, the discrepancy in the resistance between the experimental results and the theoretical projection in our study is considered to be something else.

First, there is a report on interfacial roughening during solid phase epitaxy [28]. Since the dose used in our experiment is over the critical dose, which is somewhere between 6×10^{13} /cm^2 to 1×10^{14} /cm^2 for FIB [29], solid phase epitaxy would occur and induce the interfacial roughening. Second, from the experimental results in Section 4.2, it is considered that the residue defects exist, which would affect the electrons transport. Third, with the small enough line width, it might be possible that the shape of the structure affect the electrons transport.

In our opinion, it is likely that the higher than expected resistance was caused by the combined effect of interfacial roughness, the residue damages, and the shape of the structure. In a wider channel, carriers can find a path to go from one point to another point, even though there are residue damages to obstruct the

transport. However, in a narrow channel like in this case, some carriers might have difficulty to find the path between the channel boundary and the defects region. Moreover, the carriers that found the path might have difficulty in transport due to the interfacial roughness. In brief, this might be considered as multiple resisters connected to each other in series with few of them have very high resistance, which would be the bottleneck of the circuit. More investigation is necessary to explain this phenomenon.

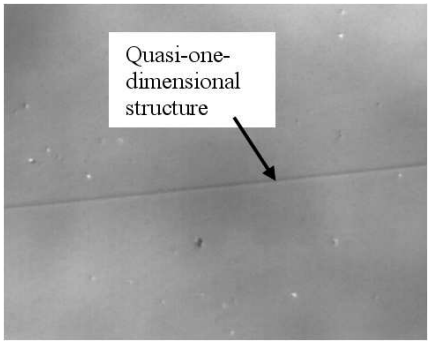

Fig.8: *Surface topography of the narrow line structure.*

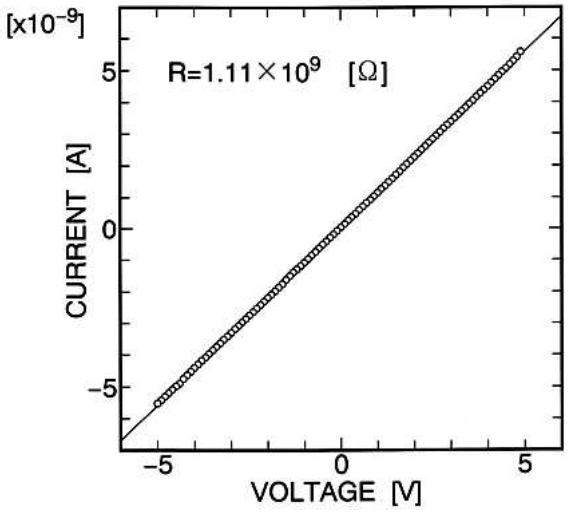

Fig.9: *$I-V$ characteristics of the narrow line structure.*

5. CONCLUSION

Shallow p+-n junctions fabricated by 20-keV Ga^+ FIB on Si substrate, both on-axis implantation and 7 °off-axis implantation, were successfully formed without masks. This technique has many benefits, and can be used to complement the conventional ion implantation technique in some area such as channel doping. From LSS theory, the junction depth is projected to be 45 nm. However, the results from stain method showed that the junction depth of the p^+-n junctions is 560 nm for on-axis implantation, and 410 nm for 7 ° off-axis implantation. The distribution profile of dopant from SIMS showed long tails for both as-implant and annealed specimens, which is quite different from LSS theory. Based on our detailed investigation, the discrepancies are considered to arise from the fact that the LSS theory, which does not include electronic stopping model properly, cannot provide good prediction to channeling effects. Moreover, sputtering of the top layer of samples, enhanced diffusion due to heat generated by high beam current density and also the interaction with point defects, secondary channeling effects due to low implant energy, and low carrier concentration of the substrate, are considered to play roles in the long tail of the distribution profile, which could not be predicted by the LSS theory as well. Although there were discussions about the discrepancies before [30], they did not take account of low beam energy and unique side effects caused by FIB like in our study.

The results from Hall effect measurement showed that the carrier concentration is 2.9×10^{17} /cm^3, the resistivity is 0.16 Ω-cm and the Hall drift mobility is 131 cm^2 / V-sec which is 62% of the prejected value. The residual defects are considered to be the cause of the lower than expected mobility. In our study, the detailed analysis of the $I-V$ characteristics, including the linearity at very low forward voltage, was performed. The results indicated that p-n junctions were successfully formed. The shape of the $I-V$ characteristics showed four distinct regions in the forward bias, and rising saturation current in the reverse bias. This is the first time that each region of $I-V$ characteristics of p-n junctions formed by FIB has been studied in such details. The high leakage current is considered to be the results of residual defects after annealing. Better annealing technique might help alleviate this problem.

For the first time, a narrow line was also successfully fabricated without masks by FIB. The resistance of the quasi-one-dimensional structure, was 1.1×10^9 Ω, which is 647 times higher than the projected value. Since the width of the structure is too large for quantum effects to happen, the cause might be the combined effects of interfacial roughness, the residue damages, and the shape of the structure. This result provided more insight into the characteristics of layers implanted by FIB. Further investigation is necessary to explain this phenomenon. Table 3 summarizes the achievements and contributions of this study to microelectronics field comparing to other previous work.

6. ACKNOWLEDGMENT

I would like to express my deep appreciation to Prof. H. Matsunami and all members of Matsunami Laboratory for very fruitful discussion and providing equipments used in this research.

Table 3: *Achievements and contributions of this study.*

Previous study	Our study
1. Conventional ion implantation technique needs masks.	1. FIB can perform ion implantation without masks.
2. Discrepancies between actual distribution profiles and theory have never been discussed thoroughly.	2. A detailed discussion about the discrepancies was done.
3. Discussion on each region of the $I-V$ characteristics of p-n junctions formed by FIB has never been done.	3. A study on each region of the $I-V$ characteristics was successfully done.
4. Investigation on the resistance of quasi-one-dimensional structure formed by FIB has never been done.	4. A successful investigation was done on the resistance characteristics of the structure.

References

[1] R. H. Dennard, F. H. Yu, V. L. Rideout, E. Bassous, and A. R. LeBlac, "Design of Ion-Implanted MOSFET's with Very Small Physical Dimensions," *IEEE Journal of Solid-State Circuits*, Vol. 9, No. 5, pp. 256-268, 1974.

[2] G. Baccarani, M. R. Wordeman, and R. H. Dennard, "Generalized Scaling Theory and Its Application to a 1/4 Micrometer MOSFET Design," *IEEE Transactions of Electron Devices*, Vol. 31, No. 4, pp. 452-462, 1984.

[3] C-M Lin and A. J. Steckl, "Si p^+-n Shallow Junction Using On-Axis Ga^+ Implantation," *Applied Physics Letters*, Vol. 52, No. 24, pp. 2049-2051, 1988.

[4] Shin Nam Hong, Gary A. Ruggles, Jimmie J. Wortman, Mehmet C. Ozturk, "Material and Electrical Properties of Ultra-Shallow p+-n Junctions Formed by Low-Energy Ion Implantation and Rapid Thermal Annealing," *IEEE Transactions on Electron Devices*, Vol. 38, No. 3, pp.476-486, 1991.

[5] H. Matsuoka, T. Ichiguchi, T. Yoshimura, and E. Takeda, "Mobility Modulation in a Quasi-One-Dimensional Si-MOSFET with a Dual-Gate Structure," *IEEE Electron Device Letters*, Vol. 13, No. 1, pp. 20-22, 1992.

[6] J. Tanaka, A. Sawada, "Simulation of a High Performance MOSFET with a Quantum Wire Structure Incorporating a Periodically Bent Si-SiO2 Interface," *IEEE Transactions on Electron Devices*, Vol. 43, No. 12, pp. 2185-2189, 1996.

[7] C. C. Shen, J. Murguia, N. Goldsman, M. Peckerar, J. Melngailis, and D. A. Antoniadis, "Use of Focused-Ion-Beam and Modeling to Optimize Submicron MOSFET Characteristics," *IEEE Transactions on Electron Devices*, Vol. 45, No. 2, pp. 453-459, 1998.

[8] J. E. Murguia, M. I. Shepard, J. Melngailis, A. L. Lattes, and S. C. Munroe, "Increase in Silicon Charge Coupled Devices Speed with Focused Ion Beam Implanted Channels," *The Journal of Vacuum Science and Technology B*, Vol. 9, No. 5, pp. 2714-2717, 1991.

[9] A. J. Steckl, H. C. Mogul, and S. Mogren, "Electrical Properties of Nanometer-Scale Si p^+-n Junctions Fabricated by Low Energy Ga^+ Focused Ion Beam Implantation," *The Journal of Vacuum Science and Technology B*, Vol. 9, No. 5, pp. 2718-2721, 1991.

[10] S. W. Novak, C. W. Magee, H. C. Mogul, A. J. Steckl, and M. Pawlik, "Secondary Ion Mass Spectrometry Depth Profiling of Nanometer-Scale p^+-n Junctions Fabricated by Ga^+ Focused Ion Beam Implantation," *The Journal of Vacuum Science and Technology B*, Vol. 10, No. 1, pp. 333-335, 1992.

[11] H. Ryssel and I. Ruge, *Ion Implantation*, John Wiley & Sons, UK, 1986, pp. 5-16.

[12] J. Lindhard and M. Scharff, "Energy Dissipation by Ions in the keV Region," *Physical Review*, Vol. 124, No. 1, pp. 128-130, 1961.

[13] J. Singh, *Semiconductor Devices*, John Wiley & Sons, Inc., New York, 2001, pp. 185-191.

[14] D. K. Schroder, *Semiconductor Material and Device Characterization*, John Wiley & Sons, Inc., New Jersey, 2006, pp. 185-188.

[15] S. M. Sze, *Semiconductor Devices : Physics and Technology*, John Wiley & Sons, New York, 1985, pp. 92-96.

[16] B. G. Streetman, and Sanjay Banerjee, *Solid State Electronic Devices*, Prentice Hall International, Inc., New Jersey, 2000, pp. 211-216.

[17] Eiko Engineering, *Focused Ion Beam System User Manual*, 1995.

[18] B. G. Streetman, and Sanjay Banerjee, *Solid State Electronic Devices*, Prentice Hall International, Inc., New Jersey, 2000, pp. 226, 434.

[19] J. F. Gibbons, W. S. Johnson, and S. W. Mylroie, *Projected Range Statistics, Semiconductors and Related Materials*, Dowden, Hutchinson& Ross, Inc., Pennsylvania, 1975, pp.29.

[20] S. M. Sze and J. C. Irvin, "Resistivity, Mobility and Impurity Levels in GaAs, Ge, and Si at 300 K," *Solid-state Electronics*, Vol.11, pp. 599-602, 1968.

[21] S. H. Yang, S. J. Morris, S. Tian, K. B. Parab, and A. F. Tasch, "Monte Carlo Simulation of Arsenic Ion Implantation in (100) Single-Crystal Silicon," *IEEE Transactions on Semiconductor Manufacturing*, Vol. 9, No. 1, pp. 49-58, 1996.

[22] Y. Takamura, E. H. Kim, S. H. Jain, P. B. Griffin, and J. D. Plummer, "The Use of Laser Annealing to Reduce Parasitic Series Resistances in MOS Devices," *Proceedings of the 14^{th} International Conference on Ion Implantation Technology*, pp. 56-59, 2002.

[23] S. R. Walther, S. Mehta, J. Weeman, A. Grouillet and D. Brown, "Dopant Channeling as a

Function of Implant Angle for Low Energy Applications," *Proceedings of the 12th International Conference on Ion Implantation Technology*, pp. 126-129, 1998.

[24] S. N. Hong, G. A. Ruggles, J. J. Wortman, and M. C. Ozturk, "Material and Electrical Properties of Ultra-Shallow p^+-n Junctions Formed by Low-Energy Ion Implantation and Rapid Thermal Annealing," *IEEE Transactions on Electron Device*, Vol. 38, No. 3, pp. 476-486, 1991.

[25] P. Chantngarm, "Maskless etching of Microfabricated Structures with Low-Power Focused Ion Beam," *Proceedings of the 2007 Electrical Engineering / Electronics, Computer, Telecommunications and Information Technology (ECTI) International Conference*, pp. 194-197, 2007.

[26] S. M. Sze, *Physics of Semiconductor Devices*, John Wiley & Sons, USA, 1981, pp. 29.

[27] H. Matsuoka, T Ichiguchi, T. Yoshimura, and E. Takeda, "Mobility Modulation in a Quasi-One-Dimensional Si-MOSFET with a Dual-Gate Structure," *IEEE Transactions on Electron Device Letters*, Vol. 13, No. 1, pp. 20-22, 1992.

[28] W. Barvosa-Carter, M. J. Aziz, A. -V. Phan, T. Kaplan, and L. J. Gray, "Interfacial roughening during solid phase epitaxy: Interaction of dopant, stress, and anisotropy effects," *Journal of Applied Physics*, Vol. 96, No. 10, pp. 5462-5468, 2004.

[29] M. Tamura, S. Shukuri, Y. Wada, Y. Madokoro, and T. Ishitani, "Focused Ion Beam Implantation into Si," *Proceeding of the 12th International Symposium of Hosei University*, pp. 17-24, 1988.

[30] Steven W. Novak and Charles W. Magee, "Secondary ion mass spectrometry depth profiling of nanometer-scale p^+-n junctions fabricated by Ga^+ focused ion beam implantation," *Journal of Vacuum Science Technology B*, Vol. 10, No. 1, pp. 333-335, 1992.

Peerasak Chantngarm received the B.S. degree in Physics in 1994, and the M.Eng. degree in Electrical Engineering in 1996, both from Kyoto University, Japan. He became a lecturer in the Electronics Engineering Department, King Mongkut's Institute of Technology Ladkrabang.

Currently, he is an Assistant Professor with Electronics and Telecommunication Engineering Department, Pathumwan Institute of Technology. His research interests span broad aspects of semiconductor devices and VLSI design. He is a member of Eta Kappa Nu.